European Conference on Optical Communication (ECOC) 2022 © Optica Publishing Group 2022

Robust Pilot-aided Timing Recovery Algorithm for OQAM-based Digital Multi-band Systems

Wanzhen Guo(1), Zhaoquan Fan(1), Ziheng Zhang(1), Jiating Luo(2), Bofang Zheng(2), and Jian Zhao(1)

(1) School of Electronic and Information Engineering, South China University of Technology, Guangzhou, China, zhaojian@scut.edu.cn
(2) Huawei Technologies Co. Ltd., Shenzhen, China

Abstract *We propose the first timing recovery algorithm for OQAM-based digital multi-band (DMB) systems where Gardner, Godard and square-Gardner algorithms fail. 320-Gbit/s experiments and simulations show that OQAM-DMB using the proposed algorithm outperforms QAM-DMB using conventional algorithms and is also robust to spectral roll-off and DGD. ©2022 The Author(s)*

Introduction

Timing recovery (TR) plays an important role in coherent detection, as the prerequisite of the following butterfly filtering, phase recovery, and decoding. In TR, the timing error is extracted by the timing recovery algorithm (TRA) and fed back to adjust the clock sampling phase of the analog-to-digital converter or to digitally resample the signal. Gardner and Godard algorithms [1-4] have been widely used in QAM formats due to their simplicity and insensitivity to carrier phase. However, these two methods do not work for QAM signals with small spectral roll-off factors or fast-than-Nyquist. A square-Gardner (sGardner) method [5] was proposed to enhance the tolerance to the spectral roll-off but it has a poorer dispersion tolerance. More importantly, all these methods fail when the differential group delay (DGD) is equal to half of the symbol period. Because TR is performed before polarization demultiplexing, it should be robust to random rotation of state of polarization (RSOP) and DGD.

On the other hand, offset quadrature amplitude modulation based digital multi-band (OQAM-DMB) system [6-7] is attractive to enable higher spectral efficiency for high-speed coherent communications. In contrast to the QAM-based Nyquist DMB system which has to use a guard band to avoid spectral overlapping, OQAM can maintain the orthogonality without the guard band. However, as will be shown in this paper, conventional Gardner, Godard, and sGardner methods cannot be applied to the OQAM format. To the best of our knowledge, there is no report on the digital TRA for OQAM-DMB.

In this paper, for the first time, we propose a novel pilot-aided TRA for OQAM-DMB. This method is robust to different impairments, particularly the spectral roll-off and DGD which traditional methods are sensitive to. 320-Gbit/s experiments and simulations show that OQAM-DMB based on the proposed algorithm works properly for all spectral roll-off factors and DGD, and outperforms QAM-DMB using conventional TRAs. The digital phase-lock loop can be locked for the clock frequency offset within ±60 ppm and all initial sampling phase offset.

Principle

Fig. 1 shows OQAM-DMB with 4 subbands. When there is a timing error (TE) τ, the demultiplexed x- and y-polarization signals for subbands A and B can be written as:

$$\begin{bmatrix} s_{A,x}(t) \\ s_{A,y}(t) \end{bmatrix} = h_A(t)\cdot\sum_{n=-\infty}^{+\infty}\begin{bmatrix} s_{A,x}(n) \\ s_{A,y}(n) \end{bmatrix}\cdot h(t-nT/2-\tau)$$
$$\cdot\exp(j\omega_0\tau/2 + j\varphi(t) + j\beta_2 L\omega_0^{\,2}/8 + j\Delta\omega(t-\tau)) \quad (1\text{-}1)$$

$$\begin{bmatrix} s_{B,x}(t) \\ s_{B,y}(t) \end{bmatrix} = h_B(t)\cdot\sum_{n=-\infty}^{+\infty}\begin{bmatrix} s_{B,x}(n) \\ s_{B,y}(n) \end{bmatrix}\cdot h(t-nT/2-\tau)$$
$$\cdot\exp(-j\omega_0\tau/2 + j\varphi(t) + j\beta_2 L\omega_0^{\,2}/8 + j\Delta\omega(t-\tau)) \quad (1\text{-}2)$$

Here, we neglect the interference from adjacent subbands as it can be removed via averaging in TRA. $s_{A/B,x/y}(n)$ are real (imaginary) for odd (even) n. $h_A(t)$ and $h_B(t)$ are the Jones matrices while $h(\cdot)$ is the pulse shape. $\varphi(t)$, $\beta_2 L$, and $\Delta\omega$ are the phase noise, residual dispersion, and frequency offset respectively, which induce the same phase shift in subbands A and B as shown in Eq. (1). In contrast, TE-induced phases are opposite in these two subbands. Therefore, TE can be extracted by multiplying the pilots in subband A with the conjugate of the pilots in subband B.

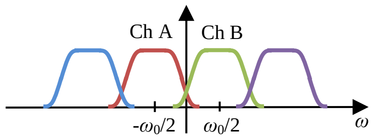

Fig. 1: Diagram of OQAM-DMB subbands. $\omega_0 = 2\pi/T$ and T is the symbol period of a subband.

However, $s_{A/B,x/y}(t)$ is still influenced by the Jones matrices $h_A(t)$ and $h_B(t)$, whose frequency-domain representations are:

$$H_A(\omega) = U_1 \begin{bmatrix} e^{j(\omega-\omega_0/2)\tau_D} & 0 \\ 0 & e^{-j(\omega-\omega_0/2)\tau_D} \end{bmatrix} U_2 \quad (2\text{-}1)$$

$$H_B(\omega) = U_1 \begin{bmatrix} e^{j(\omega+\omega_0/2)\tau_D} & 0 \\ 0 & e^{-j(\omega+\omega_0/2)\tau_D} \end{bmatrix} U_2 \quad (2\text{-}2)$$

where $2\tau_D$ is the DGD and U_1/U_2 has the form of:

$$U_i = \begin{bmatrix} c_i & d_i \\ -d_i^* & c_i^* \end{bmatrix} \quad (3)$$

where $|c_i|^2 + |d_i|^2 = 1$, i = 1 or 2. $(\cdot)^*$ represents the conjugate operation.

Tab. 1: Design of pilot symbols.

	Odd pilots	Even pilots
X-pol	P_x	$-P_y^*$
Y-pol	P_y	P_x^*

In order to enhance the tolerance to DGD and RSOP, we design the pilot symbols as shown in Tab. 1. These pilots can also be reused for other purposes, e.g. carrier phase recovery. Two types of pilots are inserted to odd/even blocks in an interleaved mode, where P_x and P_y are complex constants. Subands A and B use the same pilots.

In the transmission, the waveforms of pilots spread or even split due to the RSOP and DGD. We define the odd and even pilot waveforms of x- and y-polarization at the receiver are $A_{x,odd}$, $A_{x,even}$, $A_{y,odd}$, $A_{y,even}$ for subband A, and $B_{x,odd}$, $B_{x,even}$, $B_{y,odd}$, $B_{y,even}$ for subband B. It can be proved that the sum of the autocorrelation of $A_{x,odd}$, $A_{x,even}$, $A_{y,odd}$ and $A_{y,even}$ gives a symmetric waveform profile, and so does subband B. We then identify the locations of pilots and flip the pilot waveforms of y-polarization about their center of symmetry (CoS) for both subbands. Then we perform:

$$A_t = A_{x,odd} \cdot A'_{y,even} - A_{x,even} \cdot A'_{y,odd} \quad (4\text{-}1)$$

$$B_t = B_{x,odd} \cdot B'_{y,even} - B_{x,even} \cdot B'_{y,odd} \quad (4\text{-}2)$$

where $(\cdot)'$ represents the flipped pilot waveform about the CoS. The S-curve can be obtained by:

$$S_{TE} = \mathrm{Im}[T_e] = \mathrm{Im}[(A_t + A'_t)\cdot(B_t + B'_t)^*] \quad (5)$$

It can be proved that the T_e in Eq. (5) has a stable amplitude and a phase proportional to the TE τ, and is independent of the Jones matrices $H_A(\omega)$ and $H_B(\omega)$.

Experimental and simulation setup

Fig. 2 shows the experimental setup of a 40-Gbaud DP-16OQAM-DMB system. Four subbands were employed with 10 Gbaud per subband. Pilot symbols were designed as Tab. 1 with P_x = 3+3j and P_y = 3-3j, which were inserted into payload symbols periodically at a pilot ratio of 1/32. The optical signal-to-noise ratio (OSNR) was controlled by adjusting the attenuation of VOA1, while VOA2 was used to set the signal power into coherent receiver as -7 dBm. In the receiver DSP, as shown in Fig. 3, TE was firstly added to emulate the clock frequency offset and initial sampling phase offset. The signal with TE was demultiplexed into subbands. Subbands A and B as described in Fig. 1 were used to calculate the TE which was fed back to control the digital oscillator. A loop delay of 12.8 ns was added to emulate the hardware delay. The BER was measured after the digital phase-lock loop (DPLL) had been locked.

In order to investigate the tolerance to DGD and RSOP, we also simulated OQAM-DMB with a setup the same as Fig. 2 with varying DGD at the RSOP speed of 50 kHz.

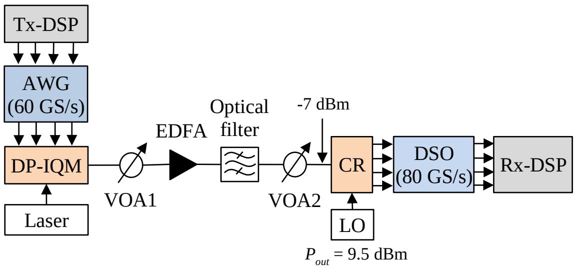

Fig. 2: Experimental setup. AWG: arbitrary waveform generator; DP-IQM: dual-polarization IQ modulator; VOA: variable optical attenuator; CR: coherent receiver; LO: local oscillator; DSO: digital storage oscilloscope.

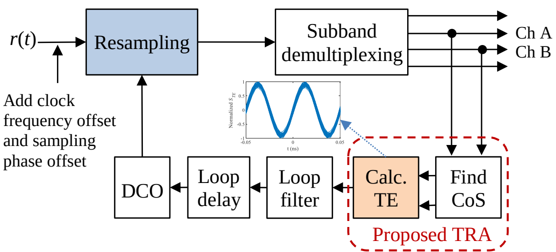

Fig. 3: Structure of the digital phase-lock loop (DPLL). CoS: center of symmetry; TE: timing error; DCO: digitally controlled oscillator. Loop delay is used to emulate the hardware delay. Inset: S-curve of the estimated TE.

Results and discussions

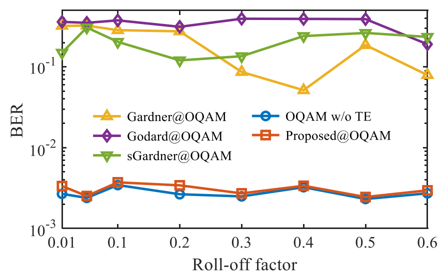

Fig. 4: BER versus the spectral roll-off for OQAM-DMB using different TR algorithms. The OSNR is 24 dB. The clock phase and frequency offset are T/6 and 20 ppm, respectively.

Fig. 4 depicts BER of OQAM-DMB using different TR algorithms. It is seen that all conventional methods including Gardner, Godard and sGardner algorithms fail, while the proposed method works properly with negligible penalty regardless of the spectral roll-off. Fig. 5 shows the convergence curve of the DPLL. It is shown that the DPLL is locked after 200 iterations. In contrast, conventional TR methods cannot obtain proper TE so that the DPLL does not converge.

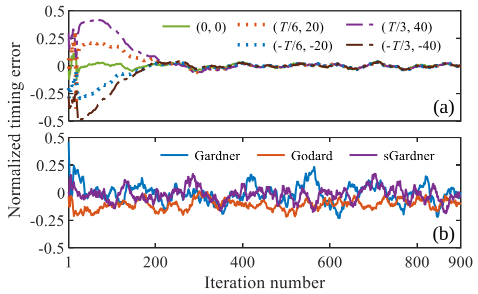

Fig. 5: Convergence curve of the DPLL for (a) the proposed method and (b) conventional methods in OQAM-DMB. (*T*/6, 20) etc. represent the initial sampling phase offset and clock frequency offset. The frequency offset unit is ppm. The initial sampling phase and frequency offset in (b) is (*T*/6, 20).

We compare the performance of OQAM-DMB using the proposed method and QAM-DMB based on the conventional algorithms, as shown in Fig. 6. It is seen that when there is no timing error, the performance of OQAM-DMB is insensitive to the spectral roll-off because it can maintain the orthogonality without guard band. In contrast, QAM-DMB requires a spectral guard band and so is degraded as the roll-off factor increases due to the bandwidth limitation effect. When TE exists, the proposed method works properly in OQAM-DMB with negligible penalty. However, in QAM-DMB, Gardner and Godard methods fail when the roll-off factor is small. sGardner works under small roll-off factors but its performance degrades for large roll-off factors.

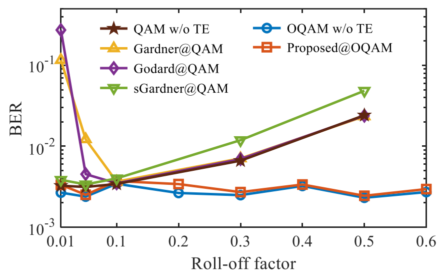

Fig. 6: BER of OQAM-DMB using the proposed method and QAM-DMB based on conventional methods at 24-dB OSNR.

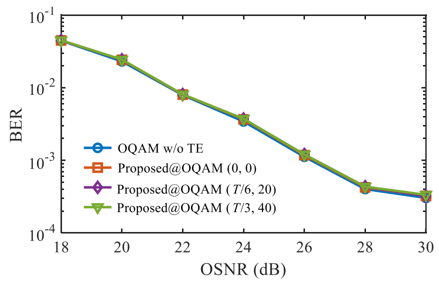

Fig. 7: BER versus OSNR for the proposed algorithm with different sampling phase offsets and clock frequency offsets.

Fig. 7 shows the BER performance of OQAM-DMB versus OSNR. It is seen that the proposed method works for all OSNRs with negligible penalty under different initial sampling phase offsets and clock frequency offsets. Fig. 8 shows the BER versus clock frequency offset under different initial sampling phase offsets. The DPLL using the proposed method converges for the clock frequency offset within ±60 ppm and all initial sampling phase offset.

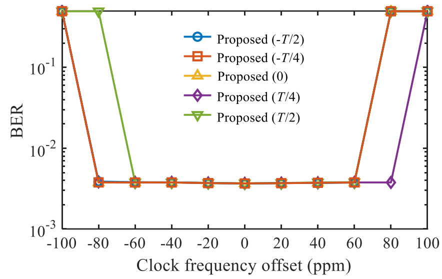

Fig. 8: BER versus clock frequency offset under different initial sampling phase offsets at 24-dB OSNR.

Finally, we simulate the tolerance to DGD, as shown in Fig. 9. Even in QAM-DMB, conventional TR algorithms cannot work when the DGD is equal to half of the symbol period. In contrast, the proposed method overcomes this shortcoming and can maintain low BERs for all DGD values.

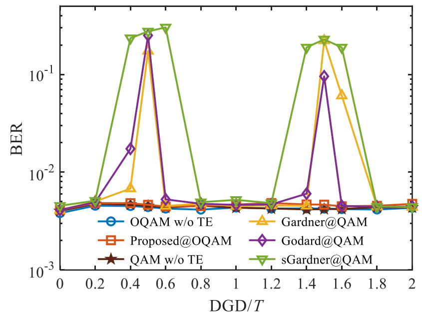

Fig. 9: Simulated BER versus DGD for OQAM-DMB based on the proposed TRA and QAM-DMB using conventional TRAs at 50-kHz RSOP speed. The sampling phase offset and clock frequency offset are *T*/2 and 40 ppm, respectively.

Conclusions

We have proposed a novel TRA for OQAM-DMB, which is robust to the spectral roll-off, OSNR, RSOP and DGD. 320-Gbit/s experiments and simulations show that OQAM-DMB using the proposed algorithm outperforms QAM-DMB with conventional TR algorithms, and the DPLL can be locked for the clock frequency offset within ±60 ppm and all initial sampling phase offset when there is a 12.8-ns loop delay.

Acknowledgments

National Natural Science Foundation of China (61971199) and Guangdong Basic and Applied Basic Research Foundation (2021A1515012309).

References

[1] D. Godard, "Passband timing recovery in an all-digital modem receiver," *IEEE Transactions on Communications*, vol. 26, no. 5, pp. 517-523, 1978. DOI: 10.1109/TCOM.1978.1094107.

[2] F. Gardner, "A BPSK/QPSK timing-error detector for sampled receivers," *IEEE Transactions on Communications*, vol. 34, no. 5, pp. 423-429, 1986. DOI: 10.1109/TCOM.1986.1096561.

[3] Arne Josten, Benedikt Bäeuerle, Edwin Dornbierer, Jonathan Boesser, David Hillerkuss, and Juerg Leuthold, "Modified Godard timing recovery for non-Integer oversampling receivers," *Applied Science*, vol. 7, no. 7, pp. 655-668, 2017. DOI: 10.3390/app7070655.

[4] Fabio A. Barbosa, Sandro M. Rossi, and Darli A. A. Mello, "Clock recovery limitations in probabilistically shaped transmission," *Optical Fiber Communication Conference* (*OFC*), paper M4J.4, 2020. DOI: 10.1364/OFC.2020.M4J.4.

[5] M. Yan, Z. Tao, L. Dou, L. Li, Y. Zhao, T. Hoshida, and J. C. Rasmussen, "Digital clock recovery algorithm for Nyquist signal," *Optical Fiber Communication Conference* (*OFC*), paper OTu2I.7, 2013. DOI: 10.1364/ofc.2013.otu2i.7.

[6] Sebastian Randel, Alberto Sierra, Xiang Liu, S. Chandrasekhar, and Peter J. Winzer, "Study of multicarrier offset-QAM for spectrally efficient coherent optical communications," *European Conference and Exhibition on Optical Communication* (*ECOC*), paper Th.11.A.1, 2011. DOI: 10.1364/ecoc.2011.th.11.a.1.

[7] Jian Zhao and Paul Townsend, "Independent component analysis for phase and residual frequency offset compensation in OQAM multicarrier systems," *IEEE Journal of Lightwave Technology*, vol. 38, no. 15, pp. 3897-3907, 2020. DOI: 10.1109/JLT.2020.2983413.